# Fully Coherent X-Ray Pulses from a Regenerative-Amplifier Free-Electron Laser

Zhirong Huang and Ronald D. Ruth

*Stanford Linear Accelerator Center, Stanford University, Stanford, California 94309, USA*

(Received 30 January 2006; published 13 April 2006)

We propose and analyze a regenerative-amplifier free-electron laser (FEL) to produce fully coherent, hard x-ray pulses. The method makes use of narrow-bandwidth Bragg crystals to form an x-ray feedback loop around a relatively short undulator. Self-amplified spontaneous emission (SASE) from the leading electron bunch in a bunch train is spectrally filtered by the Bragg reflectors and is brought back to the beginning of the undulator to interact repeatedly with subsequent bunches in the bunch train. The FEL interaction with these short bunches regeneratively amplifies the radiation intensity and broadens its spectrum, allowing for effective transmission of the x rays outside the crystal bandwidth. The spectral brightness of these x-ray pulses is about 2 to 3 orders of magnitude higher than that from a single-pass SASE FEL.

DOI: 10.1103/PhysRevLett.96.144801 PACS numbers: 41.60.Cr, 41.50.+h

An x-ray free-electron laser (FEL) based on self-amplified spontaneous emission (SASE) will lay the foundation of a next-generation ultrafast x-ray facility (see, e.g., Refs. [1,2]). Despite its full transverse coherence, a SASE x-ray FEL starts up from electron shot noise and is temporally chaotic. Two schemes have been proposed to improve the temporal coherence of a SASE FEL in a single-pass configuration. A high-gain harmonic generation FEL uses available seed lasers at ultraviolet wavelengths and reaches for shorter wavelengths through cascaded harmonic generation [3]. In this process, the ratio of electron shot noise to the laser signal is amplified by at least the square of the harmonic order and may limit its final wavelength reach to the soft x-ray region [4]. Another approach uses a two-stage SASE FEL and a monochromator between the stages [5]. The SASE FEL from the first undulator is spectrally filtered by a monochromator and is then amplified to saturation in the second undulator. This approach requires an undulator system almost twice as long as a single-stage SASE FEL.

Another seeding scheme, a regenerative-amplifier FEL (RAFEL), has been demonstrated in the infrared wavelength region [6] and discussed in the ultraviolet wavelength region [7,8]. It consists of a high-gain FEL undulator and a small optical feedback. In the hard x-ray region, perfect crystals may be used in the Bragg reflection geometry for x-ray feedback [9,10] and have been demonstrated experimentally for x-ray photon storage (see, e.g., Refs. [11,12]). In this Letter, we propose and analyze an x-ray RAFEL using narrow-bandwidth, high-reflectivity Bragg mirrors. The basic schematic is shown in Fig. 1. Three Bragg crystals are used to form a ring x-ray cavity around a relatively short undulator. Alternative backscattering geometry with a pair of crystals may also be used. SASE radiation from the leading electron bunch in a bunch train is spectrally filtered by the Bragg reflectors and is brought back to the beginning of the undulator to interact with the second bunch. This process continues bunch to bunch, yielding an exponentially growing laser field in the x-ray cavity. The FEL interaction with these short bunches regeneratively amplifies the radiation intensity and broadens its spectrum. The downstream crystal transmits the part of the radiation spectrum outside its bandwidth and feeds back the filtered radiation to continue the amplification process. Compared to a SASE x-ray FEL that typically requires more than 100 m of undulator length, this approach uses a significantly shorter undulator but a small number of electron bunches to generate multi-GW x-ray pulses with excellent temporal coherence. The resulting spectral brightness of these x-ray pulses can be another 2 to 3 orders of magnitude higher than the SASE FEL.

We first consider a one-dimensional (1D) model of the narrow-bandwidth RAFEL to describe its main characteristics such as the temporal profile, the round-trip power gain and the maximum extraction efficiency. At the beginning of the $n$th undulator pass, the radiation field is $E_n(t)$ with $t$ being the arrival time relative to the bunch center. The radiation field at the undulator end is

$$E_n^a(t) \approx E_n(t)g(t) + \delta E_n(t), \qquad (1)$$

where $\delta E_n(t)$ is the SASE signal of the $n$th electron bunch.

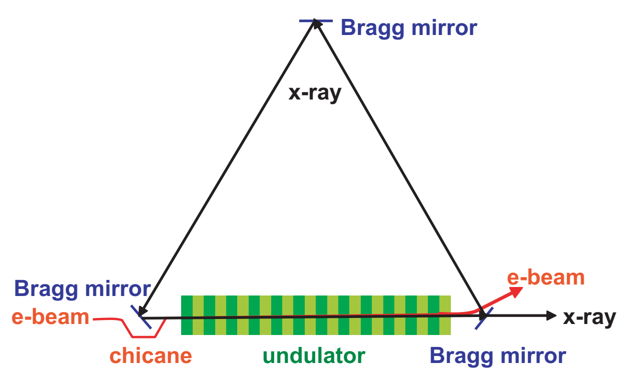


FIG. 1 (color online). Schematic of an x-ray RAFEL using three Bragg crystals.

 

When the radiation slippage length is much smaller than the electron bunch length, the radiation field gain factor $g(t)$ depends on the local bunch current. As the short undulator does not support exponential growth in a single pass, we may take $g(t) \approx g_0 \exp(-t^2/2\sigma_\tau^2)$ for a Gaussian bunch with the rms pulse duration $\sigma_\tau$. The more precise gain dependence on the current (including slippage) is used in numerical simulations shown below.

The amplified signal is then spectrally filtered by the Bragg mirrors and is fed back to the entrance of the undulator in the $(n+1)$th pass, i.e.,

$$E_{n+1}(t) = \int_{-\infty}^{\infty} \frac{d\omega}{2\pi} e^{-i\omega t} \int_{-\infty}^{\infty} dt' E_n^a(t') e^{i\omega t'} f(\omega - \omega_r), \tag{2}$$

where $f(u) = r\exp(-u^2/4\sigma_m^2)$ is a Gaussian spectral filter function with the rms intensity bandwidth $\sigma_m$, and $\omega_r$ is the central frequency of the filter with the power reflectivity $|r|^2 \leq 1$. For a high-gain amplifier after a few passes, the seed signal dominates over the SASE, so that we can neglect the second term on the right side of Eq. (1). Integrating Eq. (2) over the frequency yields

$$E_{n+1}(t) = \int_{-\infty}^{\infty} dt' \frac{r\sigma_m}{\sqrt{\pi}} e^{-i\omega_r(t-t')} e^{-\sigma_m^2(t-t')^2} g(t') E_n(t'). \tag{3}$$

Since there is no initial seed signal, $E_1(t) = 0$, and

$$E_2(t) = \int_{-\infty}^{\infty} dt' \frac{r\sigma_m}{\sqrt{\pi}} e^{-i\omega_r(t-t')} e^{-\sigma_m^2(t-t')^2} \delta E_1(t') \tag{4}$$

is the spectrally filtered SASE from the first pass that seeds the second pass.

For $n \gg 1$, we look for an exponentially growing field

$$E_n(t) = \Lambda^{n-1} A(t) e^{-i\omega_r t}. \tag{5}$$

Equation (3) is then transformed to an integral equation:

$$\Lambda A(t) = \frac{r\sigma_m}{\sqrt{\pi}} \int_{-\infty}^{\infty} dt' e^{-\sigma_m^2(t-t')^2} g(t') A(t'). \tag{6}$$

We expect that a Gaussian fundamental mode will have the largest gain $|\Lambda_0|$, i.e.,

$$A_0(t) = \exp\left(-\frac{t^2}{4\sigma_{x0}^2}\right). \tag{7}$$

Here $\sigma_{x0}$ is the rms pulse duration of the returning filtered radiation. Inserting Eq. (7) into Eq. (6), we obtain

$$\Lambda_0 \exp\left(-\frac{t^2}{4\sigma_{x0}^2}\right) = \frac{2g_0 r\sigma_m\sigma_{xa}}{\sqrt{1+4\sigma_m^2\sigma_{xa}^2}} \exp\left(-\frac{\sigma_m^2 t^2}{1+4\sigma_m^2\sigma_{xa}^2}\right), \tag{8}$$

where $\sigma_{xa} = \sigma_{x0}\sigma_\tau/\sqrt{2\sigma_{x0}^2 + \sigma_\tau^2}$ is the rms x-ray pulse duration at the undulator end [see Eq. (12)]. The self-consistent solution of Eq. (8) is

$$\sigma_{x0}^2 = \frac{1+4\sigma_m^2\sigma_{xa}^2}{4\sigma_m^2} = \frac{\sqrt{1+8\sigma_m^2\sigma_\tau^2}+1}{8\sigma_m^2},$$
$$\sigma_{xa}^2 = \frac{\sqrt{1+8\sigma_m^2\sigma_\tau^2}-1}{8\sigma_m^2}, \qquad \Lambda_0 = g_0 r \frac{2\sigma_m\sigma_{xa}}{\sqrt{1+4\sigma_m^2\sigma_{xa}^2}}. \tag{9}$$

Thus, the round-trip power gain is

$$G_{\text{eff}} \equiv |\Lambda_0|^2 = G_0 R \frac{4\sigma_m^2\sigma_{xa}^2}{1+4\sigma_m^2\sigma_{xa}^2} = G_0 R \frac{\sqrt{1+8\sigma_m^2\sigma_\tau^2}-1}{\sqrt{1+8\sigma_m^2\sigma_\tau^2}+1}. \tag{10}$$

where $G_0 = |g_0|^2$ is the peak FEL gain, and $R = |r|^2$ is the peak reflectivity of the feedback system. Regenerative amplification requires that $G_{\text{eff}} > 1$. Note that $G_{\text{eff}}$ depends on the time-bandwidth product $\sigma_m\sigma_\tau$, but not on $\sigma_m$ or $\sigma_\tau$ separately.

The filtered radiation power at the undulator entrance for $n \gg 1$ is then

$$P_n(t) = |E_n|^2 = P_0 G_{\text{eff}}^{n-1} \exp\left(-\frac{t^2}{2\sigma_{x0}^2}\right), \tag{11}$$

where $P_0$ is the effective noise power within the crystal bandwidth that starts the process. The amplified radiation at the end of the $n$th undulator pass is

$$P_n^a(t) = |E_n^a|^2 = P_0 G_0 G_{\text{eff}}^{n-1} \exp\left(-\frac{t^2}{2\sigma_{xa}^2}\right), \tag{12}$$

with $\sigma_{xa}$ given by Eq. (9). If we neglect any absorption in the crystal, the part of the radiation energy (with frequency content mainly outside the feedback bandwidth) may be transmitted with the maximum efficiency

$$\eta = \frac{\int P_n^a(t)dt - \int P_{n+1}(t)dt}{\int P_n^a(t)dt} = 1 - R\sqrt{\frac{4\sigma_m^2\sigma_{xa}^2}{1+4\sigma_m^2\sigma_{xa}^2}}. \tag{13}$$

In view of Eq. (10), the maximum extraction efficiency is also a function of the time-bandwidth product $\sigma_m\sigma_\tau$.

As a numerical example, we discuss how the proposed RAFEL might be implemented in the Linac Coherent Light Source (LCLS) [1]. The x-ray wavelength is chosen to be about 1.55 Å since diamond (400) crystals may be used at a Bragg angle $\theta_B = 60°$. The diamond (115) reflection plane may be as well chosen at 1.2 Å for the same Bragg angle. Three such crystals are necessary to form an x-ray cavity as shown in Fig. 1. The reflectivity curve of a 100 $\mu$m-thick diamond (400) crystal for the 8 keV, $\pi$-polarized radiation is shown in Fig. 2 as computed by XOP [13]. The x-ray reflectivity $R \approx (97\%)^3 \approx 91\%$ within the Darwin width $\Delta\theta_D \approx 7$ $\mu$rad, corresponding to the flattop region of Fig. 2 with $\Delta\omega_m/\omega_r = \Delta\theta_D/\tan\theta_B \approx 4 \times 10^{-6}$. The expected rms angular divergence of the FEL radiation is

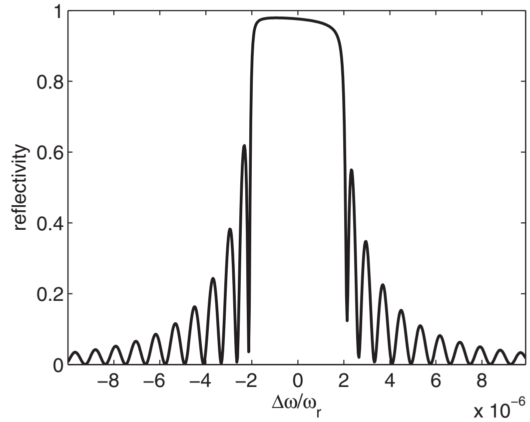


FIG. 2. X-ray reflectivity of a 100 $\mu$m-thick diamond (400) crystal for 8 keV, $\pi$-polarized radiation.

about 0.5 $\mu$rad, which is well within the Darwin width but washes out the interference fringes shown in Fig. 2. The crystals may be bent slightly to provide the necessary focusing of the filtered radiation.

In order to accelerate a long bunch train in the SLAC linac, we use the entire rf macropulse available without the rf pulse compression (SLED). The maximum LCLS linac energy, without the SLED, is about 10 GeV. Table I lists the beam and undulator parameters that are typical for x-ray FELs such as the LCLS, except that the length of the undulator is only 20 m instead of more than 100 m planned for the LCLS. We have performed a three-dimensional (3D) GENESIS [14] FEL simulation that shows the maximum power gain $G_0 \approx 39$ after the 20 m undulator, with the FWHM relative gain bandwidth about $2 \times 10^{-3}$. The LCLS accelerator and bunch compressor systems are expected to generate a bunch current profile which is more flattop than Gaussian, with a flattop duration $T = 100$ fs [1]. If we take $\sigma_\tau \approx T/2.35$ and $\sigma_m \approx \Delta\omega_m/2.35$ in Eq. (10), we obtain the round-trip gain $G_{\rm eff} \approx 16$ under these parameters.

TABLE I. Parameters for an x-ray RAFEL.

| Parameter | Symbol | Value |
|---|---|---|
| electron energy | $\gamma mc^2$ | 9.9 GeV |
| number of bunches | | 10 to 11 |
| bunch spacing | | ~0.25 $\mu$s |
| bunch charge | $Q$ | ~300 pC |
| bunch peak current | $I_{\rm pk}$ | 3 kA |
| fwhm bunch duration (flattop) | $T$ | 100 fs |
| rms energy spread at undulator | $\sigma_E/E$ | $1 \times 10^{-4}$ |
| transverse norm. emittance | $\gamma\varepsilon_{x,y}$ | 1 $\mu$m |
| undulator mean beta function | $\beta_{x,y}$ | 18 m |
| undulator period | $\lambda_u$ | 0.03 m |
| undulator parameter | $K$ | 2.4 |
| FEL wavelength | $\lambda_r$ | 1.55 Å |
| photon energy | $\hbar\omega_r$ | 8 keV |
| FEL parameter | $\rho$ | $5 \times 10^{-4}$ |
| undulator length | $L_u$ | 20 m |
| maximum FEL gain per pass | $G_0$ | 39 |
| 3-crystal bandwidth | $(\Delta\omega_m/\omega_r)$ | $4 \times 10^{-6}$ |
| 3-crystal reflectivity | $R$ | 91% |

We have developed a 1D FEL code that simulates the regenerative amplification process. The electron rms energy spread is increased in the 1D code to $3.8 \times 10^{-4}$ so that the 1D FEL gain matches the 3D FEL gain $G_0 = 39$ obtained from the GENESIS simulation. The simulation using a flattop current profile and a nearly flattop crystal reflectivity curve shows that the round-trip gain $G_{\rm eff} \approx 14$ in the exponential growth stage and that the RAFEL reaches saturation within 10 x-ray passes. For a total x-ray cavity length of 75 m (25 m for each of three cavity arms in Fig. 1), the duration of the 10-bunch train is about 2.25 $\mu$s and is within the 3.5 $\mu$s uncompressed rf pulse length after taking into account the structure filling time ($\sim 0.8$ $\mu$s). To stay well within the FEL full gain bandwidth of $2 \times 10^{-3}$, the relative energy variation of the whole bunch train should be less than $\pm 0.05\%$ and may be achieved with some beam loading compensation for the SLAC linac. A bunch-to-bunch time jitter of about $\pm 100$ fs would require a 11-bunch train of 2.5 $\mu$s in order for the FEL to reach saturation.

Figure 3 shows that the radiation energy at the undulator end is mainly the broadband SASE radiation in the first three passes or so and is then dominated by the narrow-bandwidth filtered signal up to the FEL saturation. Figure 4 shows the temporal profile of the reflected and transmitted FEL power for a 100 $\mu$m-thick diamond crystal with about 82% transmission outside the crystal bandwidth centered at 8 keV. The broadband SASE radiation transmitted through the end crystal (the noisy part of the blue solid curve in Fig. 4) can be separated from the narrow-bandwidth signal by another monochromator following the transmission as demonstrated in Fig. 5. The total x-ray energy dose absorbed by the undulator-end crystal (FEL plus spontaneous

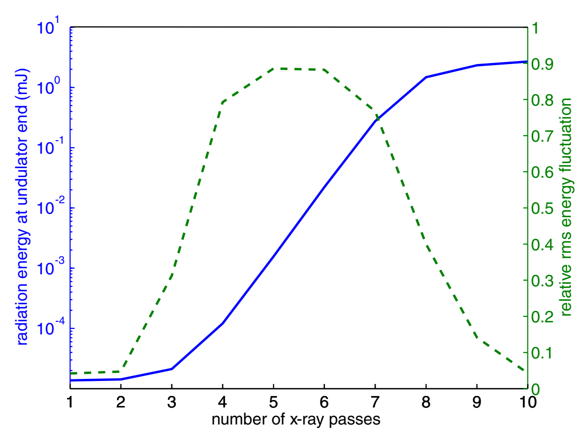


FIG. 3 (color online). Average radiated energy (blue solid line) and relative rms energy fluctuation (green dashed line) at the undulator end.

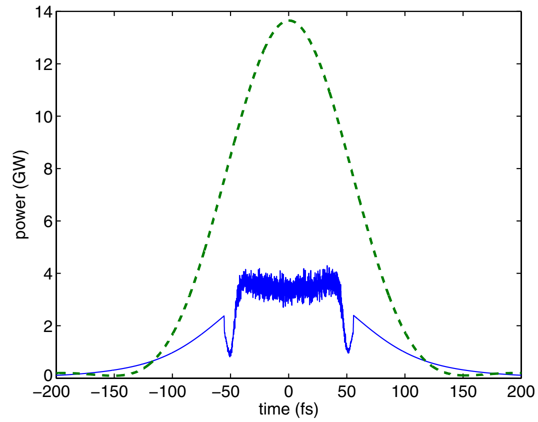


FIG. 4 (color online). Temporal profile of the reflected (green dashed line) and transmitted (blue solid line) FEL power at the end of 10th pass.

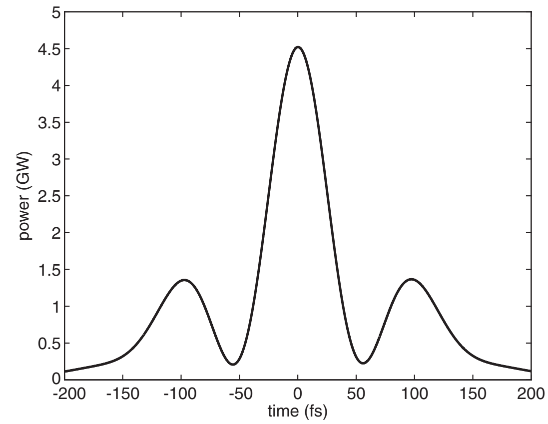


FIG. 5. Temporal profile of the final transmitted FEL power after passing a monochromator with a FWHM bandwidth $= 2\Delta\omega_m/\omega_r = 8 \times 10^{-6}$ to filter out the SASE radiation.

radiation) is estimated to be 2 orders of magnitude smaller than the melting dose level for diamond. Finally, Fig. 3 also shows that the shot-to-shot radiation energy fluctuates up to 90% in the exponential growth stage but quickly reduces to about 5% at the end of the 10th pass. Although a monochromator may also be used in a saturated SASE FEL to select a single longitudinal mode, the radiation power will be reduced by the ratio of the SASE bandwidth to the monochromator bandwidth, and the filtered radiation energy still fluctuates 100%.

While we consider a ring x-ray cavity with 60° Bragg reflection for illustration, the RAFEL scheme and its analysis presented here are equally applicable to other geometries such as a backscattered x-ray cavity with 90° Bragg reflections. The round-trip time of this cavity is only two thirds of the ring cavity shown in Fig. 1, allowing for 50% more electron bunches in a bunch train of the same duration to participate in the RAFEL process. The reflectivity at exactly 90° Bragg reflection for cubic crystals such as diamond may be complicated by multiple-wave diffraction and has not been studied here. Crystals with lower structure symmetry such as sapphire may provide the necessary high reflectivity in backscattering as demonstrated in Ref. [12].

In summary, we have described a narrow-bandwidth regenerative-amplifier FEL at the hard x-ray wavelength region using Bragg crystals that produces nearly transform limited x-ray pulses in both transverse and longitudinal dimensions. Compared to a SASE x-ray source that possesses a typical bandwidth on the order of $10^{-3}$, the bandwidth of an x-ray RAFEL can be more than 2 orders of magnitude smaller, resulting in a factor of a few hundred improvement in spectral brightness of the radiation source. The use of multiple bunches in a bunch train for regenerative amplification allows for a relatively short undulator system and may be adapted in the LCLS using the SLAC *s*-band linac. Since superconducting rf structures can support a much longer bunch train in an rf macropulse, an x-ray RAFEL based on a superconducting linac may require a much lower single-pass gain and hence relax some of beam and jitter requirements provided that the additional radiation damage to the x-ray optics is tolerable. Therefore, the method described in this Letter is a promising approach to achieve a fully coherent x-ray laser.

We thank J. Hastings, J. Als-Nielson, J. Arthur, and B. Yang for useful discussions on x-ray optics. Z. H. thanks K.-J. Kim for general discussions and for providing Refs. [9,10]. This work was supported by Department of Energy Contract No. DE-AC02-76SF00515.

[1] LCLS Conceptual Design Report No. SLAC-R-593, edited by J. Galayda, 2002.
[2] TESLA XFEL Technical Design Supplement Report No. TESLA-FEL-2002-09, edited by R. Brinkmann *et al.*, 2002.
[3] L.-H. Yu, Phys. Rev. A **44**, 5178 (1991).
[4] E. Saldin, E. Schneidmiller, and M. Yurkov, Opt. Commun. **202**, 169 (2002).
[5] J. Feldhaus *et al.*, Opt. Commun. **140**, 341 (1997).
[6] D. Nguyen *et al.*, Nucl. Instrum. Methods Phys. Res., Sect. A **429**, 125 (1999).
[7] B. Faatz *et al.*, Nucl. Instrum. Methods Phys. Res., Sect. A **429**, 424 (1999).
[8] N. Thompson, M. Poole, and B. McNeil, in *Proceedings of the 27th Free Electron Laser Conference*, econf c0508213, p. 79 (2005).
[9] R. Colella and A. Luccio, Opt. Commun. **50**, 41 (1984).
[10] B. Adams and G. Materlik, in *Proceedings of the 1996 Free Electron Lasers* (Elsevier, Amsterdam, 1997), Vol. II–24.
[11] K.-D. Liss *et al.*, Nature (London) **404**, 371 (2000).
[12] Yu. Shvyd'ko *et al.*, Phys. Rev. Lett. **90**, 013904 (2003).
[13] M. S. del Rio and R. Dejus, "XOP - X-ray Oriented Programs," http://www.esrf.fr/computing/scientific/xop/.
[14] S. Reiche, Nucl. Instrum. Methods Phys. Res., Sect. A **429**, 243 (1999).